QUARKS AND PARTONS

F.E. CLOSE
Rutherford Laboratory

PART I: QUARKS AND SPECTROSCOPY (Sections 1 and 2)

This material exists in "How high are higher symmetries ...." Rutherford Laboratory report RL-75-091 and is not reproduced here.

PART II: QUARKS IN DEEP INELASTIC PROCESSES

CONTENTS

3. Introduction

4. Inelastic Electron Scattering

5. "Derivation" of scaling in the parton model
   - 5.1 Electron scattering in Coulomb field
   - 5.2 Electron-Muon scattering
   - 5.3 Electron-Parton scattering

6. Partons = Quarks?
   - 6.1 Electromagnetic Structure Functions
   - 6.2 Comparison of electromagnetic and Neutrino Interactions
   - 6.3 Gluon Momentum
   - 6.4 Sum Rules
   - 6.5 Neutrino Interactions

7. Charm Production in νN and eN interactions

8. Electron-positron annihilation

9. Inclusive production of hadrons in the quark-parton model

10. Angular distributions of hadron in $e^+e^- \to h$ + anything

3. Introduction

The studies of inelastic electron scattering at SLAC and of neutrino scattering at CERN have been widely interpreted as giving support to the idea that the nucleon is built from elementary constituents, called partons, and that these partons have the same quantum numbers as the quarks that are familiar in spectroscopy. In particular, a very simple regularity in the data, known as scale invariance or just "scaling" was seen at least at moderate energies ($2 \lesssim E \lesssim 20$ GeV, $Q^2 \gtrsim 1$ GeV) which is natural in the parton model.

The data on e^+e^- annihilation also appear to be consistent with scaling when $E_{c.m} \lesssim 3$ GeV. Then after an energy region ($3 \lesssim E \lesssim 5$ GeV) where the new particles and a new production threshold are manifested, one again sees apparently a rescaling when $E \gtrsim 5$ GeV.

These lectures will be concerned with the scaling phenomena. Professor Wiik has discussed the new particles and related effects in e^+e^- annihilation. One may also expect the new hadronic degree of freedom (charm ?) to generate scaling violations in inelastic electron and neutrino scattering. These are mentioned briefly in these lectures and, in neutrino scattering, by Prof. Steinberger.

4. Inelastic Electron Scattering

The inelastic scattering of electrons on nucleons

$$eN \to e + \text{anything} \qquad (4.1)$$

may be represented by fig. 1 in the one-photon exchange approximation. Here k,k' are the initial and final four momenta of the leptons (energy E,E' in the lab.) and W is the mass of the produced hadronic system.

In the lab. the photon energy $\nu = E-E'$ and we can also vary its mass squared

$$q^2 = (k-k')^2 = -4EE'\sin^2\frac{\theta}{2} \qquad (4.2)$$

where θ is the lab. scattering angle of the lepton.

The lepton-photon vertex being known from QED, then the essential dynamics is in the virtual photo-absorption vertex fig. 2, which is a function of two variables ν, q^2.

We see that

$$W^2 \equiv (p+q)^2 = M^2 + 2p\cdot q + q^2 \underset{(lab.)}{=} M^2 + 2M\nu - Q^2 \qquad (4.3)$$

(where $Q^2 \equiv -q^2 \geq 0$).

We will also meet the dimensionless variable

$$\omega \equiv \frac{2M\nu}{Q^2} \qquad (4.4)$$

The region of ν, Q^2 accessible in the electron scattering is shown in fig. 3. Lines of fixed ω radiate from the origin ranging from $\omega = 1$ (elastic scattering) to $\omega = \infty$. Fixed W is also exhibited.

For $Q^2 = 0$ the photon has helicity ± 1 only ("transverse"). For $Q^2 \neq 0$ both transverse and longitudinal (helicity zero) degree of freedom are present. Hence the scattering cross-section involves two structure functions $W_{1,2}(\nu, Q^2)$

$$\frac{d^2\sigma}{dQ^2 d\nu} = \frac{E'}{E}\frac{4\pi\alpha^2}{Q^4}\left\{\cos^2\frac{\theta}{2} W_2(\nu,Q^2) + 2\sin^2\frac{\theta}{2} W_1(\nu,Q^2)\right\} \qquad (4.5)$$

which are related to the two virtual photo-absorption cross sections by

$$W_1(Q^2,\nu) = \frac{K}{4\pi^2\alpha}\sigma_T(Q^2,\nu)$$

$$W_2(Q^2,\nu) = \frac{K}{4\pi^2\alpha}\frac{Q^2}{Q^2+\nu^2}\left(\sigma_T(Q^2,\nu) + \sigma_L(Q^2,\nu)\right) \qquad (4.6)$$

with $K \equiv \nu - Q^2/2M$ the virtual photon flux.

For fixed W (e.g. $\Delta(1236)$)

$$\begin{matrix} MW_1(Q^2,W) \\ \nu W_2(Q^2,W) \end{matrix} \xrightarrow{Q^2\to\infty} 0$$

due to the resonance form factors killing the cross-section at large Q^2. However, for fixed $\omega \equiv 2M\nu/Q^2$ we find the remarkable phenomenon that (for $Q^2 \gtrsim 1$ GeV^2)

$$MW_1(\omega, Q^2) \longrightarrow F_1(\omega) \qquad (4.9)$$

$$\nu W_2(\omega, Q^2) \longrightarrow F_2(\omega) \qquad (4.10)$$

independent of Q^2 ("Scaling"). The Q^2 independence of νW_2 for ep → e + anything is seen at $\omega = 4$ in fig. 4. This phenomenon, together with the fact that (fig. 5)

$$\frac{\sigma_L}{\sigma_T} \simeq \frac{\omega F_2 - F_1}{2F_1} \simeq 0 \qquad (4.11)$$

suggests a simple spin $\frac{1}{2}$ parton substructure in the target.

For the basic scattering of the electron being on a parton carrying fraction x of the target four momentum (fig. 6), then if the parton mass and transverse momenta are negligible one has

$$\nu W_2(\nu,Q^2) \to F_2(\omega) = \sum_i \int dx\, e_i^2 x f_i(x)\,\delta\left(x - \frac{1}{\omega}\right) \qquad (4.12)$$

where the sum is over the various species of parton (u,d,s,c ...), $f_i(x)$ is the probability that the parton has momentum in interval $x \to x + dx$. The important structure here is the $xf(x)$ structure from which many relations will be seen to flow. We shall derive this result in a moment. First let us see physically why σ_L/σ_T yields information on the parton spin.

If one sets in a frame where photon and parton momenta are collinear then a spin 0 parton could not absorb a photon with helicity ± 1. Hence for spin zero partons $\frac{\sigma_L}{\sigma_T} \to \infty$. This is not at all like the data so very little, if any, charge of the proton is carried by spin zero objects (at least for the range of $x \gtrsim 0.1$ so far studied). Spin $\frac{1}{2}$ partons give $\sigma_L/\sigma_T \simeq 0$, on the other hand. This agrees well with the data. We shall derive these results in the next paragraphs.

5. "Derivation" of Scaling in the Parton Model

5.1 Electron scattering in a Coulomb field

We shall begin by studying some QED processes. Consider first the simple case of high energy electron scattering in a Coulomb field fig. 7. Then

$$\frac{d\sigma}{dt} = \frac{4\pi\alpha^2}{t^2}\left(\frac{1+\cos\theta}{2}\right)^2 \qquad (5.1)$$

where $t \equiv -Q^2$, θ is the lab. scattering angle, stu are the Mandelstam variables. One can qualitatively understand this result:

i) the dimensions of $\frac{d\sigma}{dt}$ are E^{-4}. Since the photon propagator provides t^{-2} in $\frac{d\sigma}{dt}$ then no further dimensional quantities occur.

ii) the high energy electron-photon vertex conserves helicity. Hence 180° scattering is forbidden and in turn this is the origin of the angular dependence in eq.

5.2 Electron-muon scattering

Now we shall progress to $e^-\mu^+ \to e^-\mu^+$, fig. 8 where $s = (p_e+p_\mu)^2 = 2ME$; $u = (p_{e'}-p_\mu)^2 = -2ME'$

$$\frac{-u}{s} \simeq \frac{1+\cos\theta}{2}$$

Here

$$\frac{d\sigma}{dt} = \frac{1}{2}\,\frac{4\pi\alpha^2}{t^2}\left(\frac{u^2}{s^2}+1\right) \qquad (6.2)$$

i) the factor $\frac{1}{2}$ arises due to the averaging over the two spin states of the "target" muon (contrast the previous example)

ii) when $e^-\mu^+$ have net $J_z = \pm 1$ the 180° scattering is forbidden as before - hence the U^2/S^2. When $J_z = 0$ the 180° scattering can occur (contrast the previous example) - hence the presence of an isotropic term.

Actually we should make explicit the energy-momentum conservation. Let us do this by writing

$$\frac{d^2\sigma}{dt\,du} = \frac{1}{2}\,\frac{4\pi\alpha^2}{t^2}\left(\frac{u^2+s^2}{s^2}\right)\delta(u+t+s) \qquad (5.3)$$

(recall $s + t + u = \Sigma m^2$ and so at high energy, neglecting the masses we have $u = -(s + t)$). Now

$$s = (p_e+p_\mu)^2 \overset{\text{lab.}}{=\!=} 2ME \quad (E = E_{e^-};\ m = m_\mu) \qquad (5.4)$$

$$t = (p_e-p_{e'})^2 = -Q^2 \qquad (5.5)$$

$$u = (p_\mu-p_{e'})^2 = -2ME' \qquad (5.6)$$

so $s + t + u = 2m(E-E') - Q^2 = 2M\nu - Q^2$

It will also be useful, later, to notice that

$$\frac{-t}{s+u} = \frac{Q^2}{2M\nu} = \frac{1}{\omega} \qquad (5.7)$$

5.3 Electron-parton scattering

In the parton model, the inelastic electron-target scattering is hypothesised to be due to the elastic scattering of electrons on the partons in the target. If the partons have spin $\frac{1}{2}$ and couple to the photon just as does the μ^+ of the previous example ("pointlike coupling") then we can easily obtain an expression for the cross-section.

Let us neglect any parton momentum transverse to the target so that

$$p_{parton} = x\,p_{target} \qquad (5.8)$$

Then from the previous example we can write the cross section for elastic scattering on a muon (parton) with momentum Xp as (noting that $s \to Xs$, $u \to Xs$ but t remains untouched since this can be defined involving the electron vertex alone)

$$\left(\frac{d^2\sigma}{dt\,du}\right)_{e\mu(x)\to e\mu(x)} = \frac{1}{2}\,\frac{4\pi\alpha^2}{t^2}\,\frac{u^2+s^2}{s^2} \times \delta\big(t+x(s+u)\big) \qquad (5.9)$$

If the target is built from partons of types (flavours) labelled i, and the probability for a parton i to have momentum fraction x to x + dx is $f_i(x)$ then the inelastic e-target cross-section will be, after summing over all the elastic parton contributions

$$\left(\frac{d^2\sigma}{dt\,du}\right)_{eN\to eX} = \frac{1}{2}\frac{4\pi\alpha^2}{t^2}\frac{u^2+s^2}{s^2}\int dx \sum_i x f_i(x)\frac{1}{s+u}\,\delta\left(x-\frac{1}{\omega}\right) \qquad (5.10)$$

We already see the appearance of the structure in eq. (4.12). To obtain that expression explicitly we must compare the equation (5.10) with the expression for eN → eX which involves $W_{1,2}$ (eq. 4.5).

Noting that

$$\sin^2\frac{\theta}{2} = \frac{tm^2}{su} \quad ; \quad \frac{\epsilon'}{\epsilon} \equiv -\frac{u}{s} \qquad (5.11)$$

$$\nu = \frac{s+u}{2m} \quad ; \quad x \equiv \frac{Q^2}{2M\nu} = -\frac{t}{s+u}$$

we can manipulate eq. (2.5) into the form

$$\left(\frac{d^2\sigma}{dt\,du}\right)_{eN\to eX} = \frac{1}{2}\frac{4\pi\alpha^2}{t^2}\frac{1}{s^2(s+u)}\left[2xF_1(s+u)^2 - 2usF_2\right] \qquad (6.12)$$

where $F_1 \equiv MW_1$, $F_2 \equiv \nu W_2$

Since s and u can be independently varied we compare coefficients and immediately see that

$$2xF_1(x) = F_2(x) = \sum_i e_i^2 x f_i(x) \qquad \left(x \equiv 1/\omega\right) \qquad (5.13)$$

which is the master formula of the spin ½ parton model.

6. Partons = Quarks?

6.1 Electromagnetic structure functions

We have from eq. (3.13) that

$$F_2(x) = \sum_i e_i^2 x f_i(x) \equiv \sum_i e_i^2 q_i(x) \qquad (6.1)$$

Hence

$$F_2^{\gamma p}(x) = \frac{4}{9}\left(u^p(x)+\bar{u}^p(x)\right) + \frac{1}{9}\left(d^p(x)+\bar{d}^p(x)\right) + \frac{1}{9}\left(s^p(x)+\bar{s}^p(x)\right) \qquad (6.2)$$

$$F_2^{\gamma N}(x) = \frac{4}{9}\left(u^N(x)+\bar{u}^N(x)\right) + \frac{1}{9}\left(d^N(x) + \cdots\right)$$

Now use isospin reflection to note

$$u^p \equiv d^N \text{ (call it simply u)} \qquad (6.3)$$

$$d^p \equiv u^N \text{ (call it d)} \qquad (6.4)$$

$$s^p \equiv s^N \text{ (call it s)} \qquad (6.5)$$

with analogous constraints for the antiquarks.

Consequently

$$F_2^{\gamma p} = \frac{4}{9}\left(u+\bar{u}\right) + \frac{1}{9}\left(d+\bar{d}\right) + \frac{1}{9}\left(s+\bar{s}\right) \qquad (6.6)$$

$$F_2^{\gamma N} = \frac{4}{9}\left(d+\bar{d}\right) + \frac{1}{9}\left(u+\bar{u}\right) + \frac{1}{9}\left(s+\bar{s}\right) \qquad (6.7)$$

and so

$$\frac{1}{4} \leq \frac{F_2^{\gamma N}}{F_2^{\gamma p}}(x) \leq 4 \qquad (6.8)$$

These bounds are consistent with the data (fig.10).

We can go further by imposing ideas rooted in duality. Separate the quarks (partons) into three "valence" quarks and a sea of quarks and antiquarks along the following lines

3 valence quarks	+	Sea of $q\bar{q}$
↕		↕
Resonances	+	Background
↕		↕
Non Diffractive	+	Diffractive

Then (following e.g. Kuti-Weisskopf or Landshoff-Polkinghorne) write

$$q(x) \equiv q_V(x) + q_S(x) \qquad (6.9)$$

The original guess was

$$u_v(x) = 2d_v(x) \qquad (6.10)$$

$$s_v(x) = \bar{u}_v(x) = \bar{d}_v(x) = \bar{s}_v(x) = 0 \qquad (6.11)$$

$$u_s(x) = \bar{u}_s(x) = d_s = \bar{d}_s = s = \bar{s} \equiv K \qquad (6.12)$$

This gives

$$F_2^{\gamma N} = \frac{1}{9}\left(u_v + 4d_v\right) + \frac{12}{9}K \qquad (6.13)$$

$$F_2^{\gamma P} = \frac{1}{9}\left(d_v + 4u_v\right) + \frac{12}{9}K \qquad (6.14)$$

so that if K(x) dominates

$$\frac{F_2^{\gamma N}}{F_2^{\gamma P}}(x) \to 1 \qquad (x \to 0\ ?) \qquad (6.15)$$

whereas for dominance of the valence quarks (and if $u_v \geq 2d_v$)

$$\frac{F_2^{\gamma N}}{F_2^{\gamma P}}(x) \to \frac{2}{3} \text{ to } \frac{1}{4} \qquad (x \gtrsim 0.2\ ?) \qquad (6.16)$$

Hence we begin to have the first hints that maybe the valence quarks are dominantly at large X while the sea is near X ≃ 0. This will be reinforced in our subsequent data analyses, but first let us give an intuitive picture of why this picture is not unreasonable.

In QED the bare electron becomes dressed by diagrams such as fig. 11. The analogue for the partons will be that vector (?) gluons (something has to hold the target together) will play the role of the photons in QED. Then a three valence quark system will be dressed in fig. 12, where the wiggly lines denote gluons and the solid lines are quark-partons. The bremmstrahlung probability for momentum k in the gluon behaves as $\frac{dk}{k}$ and hence like $\frac{dx}{x}$. This means that the gluon emission, and hence the $q\bar{q}$ structure or sea, tends to like small x. So we can view the target as three valence quarks carrying most of the momentum bound by gluons which will also carry momentum and radiating and absorbing soft gluons which dress the valence quarks with a soft cloud of $q\bar{q}$ pairs.

6.2 Comparison of electromagnetic and neutrino interactions

The charged weak interaction couples to the isospin of the partons and in the limit of zero Cabibbo angle the reaction is triggered by

$$\nu\begin{bmatrix} d \\ \bar{u} \end{bmatrix} \to \mu^-\begin{bmatrix} u \\ \bar{d} \end{bmatrix} \qquad (6.17)$$

we have

$$F_2^{\nu P}(x) = 2\left[d(x) + \bar{u}(x)\right] \qquad (6.18)$$

$$F_2^{\nu N}(x) = 2\left[u(x) + \bar{d}(x)\right] \qquad (6.19)$$

where in (6.19) we have used $d^N = u^P = u$ etc. The factor of 2 arises from the presence of axial as well as vector currents coupling and in the parton model the weak current is taken to be V - A as for leptons, hence the axial coupling magnitude is the same as that of the vector.

Comparing (6.18, 6.19) with (6.6, 6.7) yields

$$\left[\frac{F_2^{\gamma N} + F_2^{\gamma P}}{F_2^{\nu N} + F_2^{\nu P}}\right](x) = \frac{\frac{5}{9}\left(u+\bar{u}+d+\bar{d}\right) + \frac{2}{9}\left(s+\bar{s}\right)}{2\left(u+\bar{u}+d+\bar{d}\right)} \geq \frac{5}{18} \qquad (6.20)$$

(the rather mysterious $5/18$ is of course just the average squared charge of the u, d quarks).

In fig. 13 we see the data from CERN-Gargamelle where $F_2^{\nu N+\nu P}(x)$ is compared with $\frac{18}{5}\,F_2^{eP+eN}$ from SLAC. The agreement supports the quark quantum numbers and the saturation of the inequality at large x suggest that $s, \bar{s}$ $(x \gtrsim 0.2) \simeq 0$ (which is in line with our picture that strange quarks are in the $q\bar{q}$ sea which in turn is confined to small x values).

6.3 Gluon momentum

Since $F_2(x) \sim xf(x) \sim q(x)$ then $q(x)$ is proportional to the fractional momentum distribution of the quarks. Momentum conservation then yields

$$\int_0^1 dx \left(u+\bar{u}+d+\bar{d}+s+\bar{s}\right)(x) = 1-\epsilon \qquad (6.21)$$

where ϵ will be the fraction of momentum carried by target constituents other than the quarks, e.g. the gluons.

From equations (6.6), (6.7) and (6.18, 6.19) we see that (6.21) can be rewritten as

$$\int_0^1 dx \left(\frac{9}{2}F_2^{\gamma p+\gamma n} - \frac{3}{4}F_2^{\nu p+\nu n}\right) = 1-\epsilon \qquad (6.22)$$

Inserting the data on the left hand side we find $\epsilon \simeq \frac{1}{2}$, i.e. about half the momentum is carried by the gluons.

6.4 Sum rules

Since a nucleon has no strangeness then

$$0 = \int_0^1 \frac{dx}{x}\left(s(x) - \bar{s}(x)\right) \qquad (6.23)$$

The charges of proton and neutron give

$$1 = \int \frac{dx}{x}\left(\tfrac{2}{3}(u-\bar{u}) - \tfrac{1}{3}(d-\bar{d})\right)(x)$$

$$0 = \int \frac{dx}{x}\left(\tfrac{2}{3}(d-\bar{d}) - \tfrac{1}{3}(u-\bar{u})\right)(x)$$

and so

$$2 = \int \frac{dx}{x}\left(u(x) - \bar{u}(x)\right) \qquad (6.24)$$

$$1 = \int \frac{dx}{x}\left(d(x) - \bar{d}(x)\right) \qquad (6.25)$$

These state the net number of s, d, u quarks in the proton are 0, 1, 2 respectively.

These sum rules for the quark distributions can now be combined with the structure functions relations (6.6, 6.7, 6.18, 6.19) to yield sum rules for the targets.

First, since $F_2^{\nu N}(x) - F_2^{\nu P}(x) \equiv 2\{u - \bar{u} - d + \bar{d}\}(x)$ we find the "Adler Sum Rule"

$$\int \frac{dx}{x}\left(F_2^{\nu N}(x) - F_2^{\nu P}(x)\right) = 2 \qquad (6.26)$$

Another interesting quantity is

$$F_2^{eP}(x) - F_2^{eN}(x) \equiv \frac{1}{3}\left\{u+\bar{u}-d-\bar{d}\right\}(x) \qquad (6.27)$$

If we impose duality (i.e. $u = u_v + u_s$ etc.) then the sum rules (4.24) and (4.25) become

$$1 = \int \frac{dx}{x} d_v(x) \qquad (6.28)$$

$$2 = \int \frac{dx}{x} u_v(x) \qquad (6.29)$$

and so eq. (4.27) yields

$$\left(F_2^{eP} - F_2^{eN}\right)(x) \equiv \frac{1}{3}\left\{u_v(x) - d_v(x)\right\} \qquad (6.30)$$

which gives

$$\int \frac{dx}{x}\left(F_2^{eP}(x) - F_2^{eN}(x)\right) = \frac{1}{3}\left(\equiv \sum e_p^2 - e_N^2\right) \qquad (6.31)$$

The data are consistent with this and yield 0.28 ± ?. The ? is the contribution from large (small x). If we believe that $F^{eP} - F^{eN} \sim X^{\frac{1}{2}}$ as X 10 (Regge like) then the data are consistent with the predicted value of $\frac{1}{3}$.

6.5 Neutrino interactions

Defining $x \equiv Q^2/2M\nu$ and $y = \nu/E$ then it is a straightforward exercise to rewrite eq. (4.24) in the form

$$\frac{d^2\sigma}{dx\,dy} = \frac{4\pi\alpha^2 s}{t^2}\left\{F_2(x)(1-y) + F_1(x)xy^2\right\} \qquad (6.32)$$

For the process $\nu(\bar{\nu})p \to \mu^{\pm} X$ one has a similar formula

$$\frac{d^2\sigma^{\nu,\bar{\nu}}}{dxdy} = \frac{G^2}{2\pi} s\left\{F_2(x)(1-y) + F_1(x)xy^2 \mp y\left(1-\frac{y}{2}\right)xF_3(x)\right\} \qquad (6.33)$$

in which, for spin $\frac{1}{2}$ partons, inserting $xF_1(x) = F_2(x)$ yields

$$\frac{d^2\sigma^{(\bar{\nu})}}{dxdy} = \frac{G^2}{2\pi} sF_2(x)\left\{\frac{1+(1-y)^2}{2} \mp \frac{1-(1-y)^2}{2}\frac{xF_3(x)}{F_2(x)}\right\} \qquad (6.34)$$

In comparison with the electromagnetic case, eq. (6.32), we see the absence of t^{-2} due to the assumed pointlike (no photon exchanged) nature of the neutrino interaction. Also there is the new structure function F_3 which is due to the violation of parity in the weak interactions. Its role will be transparent after we discuss the quark parton model for this process.

In the quark parton model the basic interaction is a weak coupling of lepton with the weak quark current. If the quark weak current is V - A ((like $\nu \to \mu$) then the y dependence of neutrino - quark cross-sections are as follows

$$\frac{d\sigma}{dy}\left[\nu q; \bar{\nu}\bar{q}\right] \sim (1-y)^2 \qquad (6.35)$$

$$\frac{d\sigma}{dy}\left[\nu q; \bar{\nu}\bar{q}\right] \sim 1 \text{ (isotropic)} \qquad (6.36)$$

Qualitatively this can be understood as follows. For an interaction at a point one is in S wave; all the angular momentum information of the νq interaction will therefore be contained in the spin structure. A neutrino-quark interaction will have $J_z = 0$ in the c.m. system since both are carrying helicity minus one. The pointlike interaction will therefore carry no memory of direction and hence an isotropic distribution can ensue. For neutrino interacting with an antiquark, whose helicity will be plus one, the total $J_z = -1$. The emerging $\bar{q}$ and μ are right handed and left handed respectively and so $J_{z1} = -1$ along the z^1 axis (oriented at θ with respect to the initial z axis). The 180° scattering is clearly supressed and so one can appreciate the $(1-y)^2$ as against isotropic behaviour in the νq case.

For the case of an isoscalar target, writing $q(x)$ and $\bar{q}(x)$ for the probabilities to find quarks or antiquarks at given x, then

$$\frac{d^2\sigma^{\nu}}{dxdy} \sim x\left\{q(x) + (1-y)^2\bar{q}(x)\right\} \qquad (6.37)$$

$$\frac{d^2\sigma^{\bar{\nu}}}{dxdy} \sim x\left\{\bar{q}(x) + (1-y)^2 q(x)\right\} \qquad (6.38)$$

where we have used (6.35 and (6.36). Comparing with (6.34) then we have

$$\frac{xF_3(x)}{F_2(x)} = \frac{q(x) - \bar{q}(x)}{q(x) + \bar{q}(x)} \qquad (6.39)$$

and so the x distribution of quarks and antiquarks can be compared (more correctly, the distribution of V ± A elementary currents). The eq. (6.39) also helps us to appreciate why the extra structure function F_3 appears in the weak interaction as compared to the electromagnetic case. The parity violation causes the left and right handed couplings to be independent (hence F_3) in the weak interaction, and hence the difference in q and $\bar{q}$ couplings.

The data on F_2 and xF_3 from Gargamelle ($Q^2 > 1$ GeV^2, $W^2 > 4$ GeV^2) are shown in fig. 16. We see that for $x \gtrsim 0.4$ $F_2(x) \simeq xF_3(x)$ and so from eq. (4.39) we have

$$x \gtrsim 0.4 \qquad \frac{\bar{q}(x)}{q(x)} \to 0 \qquad (6.40)$$

whereas for $x \to 0$ $xF_3(x) \to 0$ and hence

$$x \to 0 \qquad \bar{q}(x) \to q(x) \qquad (6.41)$$

This fits in with our previous guess from the electromagnetic case, namely that the (valence) quarks dominate as $x \gtrsim 0.4$ while antiquarks are all in the sea with $x \to 0$.

We can look at this in more detail by studying the y distributions for various regions of x. The data for $E\nu \lesssim 30$ GeV from Gargamelle and Fermilab are all consistent with $(1-y)^2$ distributions for $\bar{\nu}$ induced reactions and isotropy for ν interactions at large X.

A best fit to the Gargamelle data on y distributions yields

$$\mathcal{B} \equiv \frac{\langle xF_3 \rangle}{\langle F_2 \rangle} \sim 0.80 \qquad (6.42)$$

and hence

$$\frac{\langle \bar{q} \rangle}{\langle q+\bar{q} \rangle} = 0.10 \pm 0.03 \qquad (6.43)$$

So far we have just assumed that the $\nu(\bar{\nu})$ data scale analogously to their electromagnetic cousin. This we should really check. If we integrate (6.34) over dx and dy then, assuming scaling (i.e. $F_2(x,Q^2) \to F_2(x)$) we have for the total cross section

$$\sigma_{\nu}^{\bar{\nu}}(S) = \frac{G^2 S}{2\pi} \int dx\, F_2(x) \left\{ \frac{2}{3} \mp \frac{1}{3} \frac{x F_3(x)}{F_2(x)} \right\} \qquad (6.44)$$

and hence would have a linear rise with energy ($S \equiv 2ME$). This is indeed consistent with the Gargamelle data as shown in Steinberger's lectures.

Furthermore, from (6.44) and (6.39) we have

$$\frac{\sigma^{\bar{\nu}}}{\sigma^{\nu}} = \frac{\frac{1}{3} + \frac{2}{3}\left\langle \frac{\bar{q}}{q+\bar{q}} \right\rangle}{1 - \frac{2}{3}\left\langle \frac{\bar{q}}{q+\bar{q}} \right\rangle} \qquad (6.45)$$

and hence is bounded to lie between $\frac{1}{3}$ and 3. The Gargamelle data (all Q^2, W) have this ratio $\simeq 0.37$ which again fits with the dominance of quarks over antiquarks (or, rather, of left handed parton currents).

If one makes the cut $Q^2 > 1$ GeV^2, $W^2 > 4$ GeV^2 then from fitting the x,y distributions one had (eq. 4.43)

$$\left\langle \bar{q}/q+\bar{q} \right\rangle = 0.10 \pm 0.03$$

and so in eq. (4.45)

$$\frac{\sigma^{\bar{\nu}}}{\sigma^{\nu}} \simeq 0.43$$

This is slightly larger than without the Q^2,W cut and while insignificant for our present discussion may be worth bearing in mind in connection with the possible increase of $\sigma^{\bar{\nu}}/\sigma^{\nu}$ at higher energies in Fermilab. (See Steinberger's lectures).

7. Charm Production in νN and eN

In view of the possibility that a new heavy hadronic degree of freedom exists associated with a charmed quark (see Prof. Wiik and Maiani's Lectures) and that this charmed quark is believed to have weak interaction

$$\bar{\nu} c \to \mu^+ \left(d \sin\theta_c + s \cos\theta_c \right) \qquad (7.1)$$

then it is interesting to see what effect it will have on the parton model predictions.

Below threshold and for $X \gtrsim 0.1$ we have

$$\frac{d\sigma^{\nu N}}{dy} \sim \text{constant} \; ; \; \frac{d\sigma^{\bar{\nu} N}}{dy} \sim (1-y)^2 \qquad (7.2)$$

due to the absence of antiquarks. This is realised in the data, whereas at $X \lesssim 0.1$ the data is consistent with isotropy for both ν and $\bar{\nu}$.

A new threshold appears at some fixed hadronic mass W and since

$$W^2 = M^2 + 2M\nu - Q^2$$

then

$$W^2 - M^2 = 2ME y (1-x) \qquad (7.3)$$

Hence a threshold at W_{th} first appears in the x and y distributions at small x and large y. Since at large y the $\bar{\nu}N$ cross section was small below threshold $|(1-y)^2$ distribution$|$ then the threshold contributions will be more immediately apprent in $\bar{\nu}N$ than νN. However, since we do not precisely

know how the antiquark distributions behave it may be hard to separate the threshold behaviour from possible antiquark contributions filling in the large y cross-section.

The data from HPWF do appear to show some hints that something anomalous is happening in the y distributions.

Above the threshold for exciting charmed particle final states the new contributions to the cross sections arising from the GIM charm-changing current are ($\cos\theta_c \simeq 0$)

$$\Delta\sigma^{\nu N} \sim s(x) + \bar{c}(x)(1-y)^2$$
$$\Delta\sigma^{\bar{\nu}N} \sim \bar{s}(x) + c(x)(1-y)^2 \qquad (7.4)$$

and so the contributions arise entirely from quarks in the sea. The actual magnitude of $\Delta\sigma/\sigma$ below threshold will of course depend upon the distribution of the u,d,s,c quarks in the sea and of the relative importance of sea and valence quarks. Particular assumptions (SU_4 symmetric sea, SU_3 symmetric sea etc.) lead to particular predictions. There is quite an industry in this direction at present.

Another interesting idea is that there may exist right handed currents involving the quarks. In particular one idea was that there might exist (in $\cos\theta_c = 0$ approximation)

$$\bar{\nu}\bar{s} \xrightarrow{R.H.} \mu^+\bar{c} \qquad (7.5)$$

This would have an isotropic distribution and be very significant in filling in the large y domain of $\sigma^{\bar{\nu}N}(x,y)$.

The possibility that $\nu d \xrightarrow{RH} \mu^- c$ is unlikely since it involves the valence quark d and so we would naively expect a doubling of $\sigma^{\nu N}/E$ on crossing charm threshold. Any such behaviour is not apparent in the data.

In deep inelastic electroproduction (or muon production) the charm production threshold should be seen at small x where

$$\frac{\Delta\sigma}{\sigma} = \frac{\frac{4}{9}\left(c(x)+\bar{c}(x)\right)}{\frac{4}{9}\left(u(x)+\bar{u}(x)\right)+\frac{1}{9}\left(d(x)+\bar{d}(x)\right)+\frac{1}{9}\left(s(x)+\bar{s}(x)\right)} \qquad (7.6)$$

In the case of an SU_4 symmetric sea one therefore would expect that $\frac{\Delta\sigma}{\sigma} = \frac{2}{3}$. While this may be true as $Q^2 \to \infty$ (where all mass scales are probably irrelevant) presumably at finite Q^2 the charm quark will be less important (being associated typically with heavier mass scales). Hence

$$\frac{\Delta\sigma}{\sigma}(x\to 0; Q^2) = \frac{2}{3}\epsilon(Q^2) \qquad (7.7)$$
$$\epsilon \equiv \frac{c(x\to 0; Q^2)}{u,d,s(x\to 0; Q^2)} \leq 1$$

A guess for the relative importance of charm to uncharmed quarks as a function of Q^2 might be something like

$$\epsilon = \frac{M_\rho^2 + Q^2}{M_\psi^2 + Q^2}$$

which is about 5% at $Q^2 = 0$ (like estimates from VMD) rising through 50% by $Q^2 = 10$ GeV^2.

The violation of scaling reported by the Chen-Hand inelastic muon scattering experiment at Fermilab. is consistent with being above charm threshold and ϵ having a Q^2 dependence similar to eq.7.8. An explicit calculation is given in ref.CSS and comparison between it and the data shown in fig. 17.

The best place for seeing the immediate effects of a new heavy, charm, threshold is in e^+e^- annihilation, to which we now turn.

8. Electron-Positron Annihilation

Production of muon pairs via a single photon in electron-positron annihilation has cross section (where $m \equiv m_\mu$)

$$\sigma(e^+e^-\to\mu^+\mu^-)(Q^2) = \frac{4\pi\alpha^2}{3Q^2}\left(1-\frac{4m^2}{Q^2}\right)^{1/2}\left(1+\frac{2m^2}{Q^2}\right) \qquad (8.1)$$
$$\xrightarrow{Q^2 \gg m^2} \frac{4\pi\alpha^2}{3Q^2} \qquad (8.2)$$

This simple expression is a nice illustration of the pointlike nature of the interaction, the dimensions are carried entirely by the large Q^2 photon mass and no scale of length associated with the muon appears. Compare this with $e^+e^- \to p\bar{p}$ which is again production of a pair of spin $\frac{1}{2}$ particles we have (where M = proton mass)

$$\sigma(e^+e^- \to p\bar{p})(Q^2) = \frac{4\pi\alpha^2}{3Q^2}\left(1-\frac{4M^2}{Q^2}\right)^{1/2}\left(G_M^2(Q^2) + \frac{2M^2}{Q^2}G_E^2(Q^2)\right) \quad (8.3)$$

$$\xrightarrow{Q^2 \gg M^2} \frac{4\pi\alpha^2}{3Q^2}G_M^2(Q^2) \quad (8.4)$$

$$\sim \frac{4\pi\alpha^2}{3Q^2}\left(1+\frac{Q^2}{0.71\,GeV^2}\right)^{-4} \quad (8.5)$$

where the finite size of the proton is always present in the form factor dependence.

The two form factors $G_{E,M}$ ("electric and magnetic") could be thought of as the longitudinal and transverse form factors since G_E couples only to the longitudinal ($J_Z = 0$) photon while G_M couples only to the transverse ($J_z = \pm 1$). Hence for pair production of spin $\frac{1}{2}$ particles

$$\frac{\sigma_L}{\sigma_T}(Q^2) = \frac{2M^2}{Q^2}\left|\frac{G_E(Q^2)}{G_M(Q^2)}\right|^2 \xrightarrow{\text{pointlike}} \frac{2M^2}{Q^2} \quad (8.6)$$

In the parton model we expect that $e^+e^- \to$ hadrons takes place by $e^+e^- \to$ parton - antiparton and the partons then fragment into the observed hadrons by some unknown mechanism. Then at large Q^2

$$\sigma(e^+e^- \to \text{hadrons}) = \sum_{i=udsc} \sigma(e^+e^- \to q_i\bar{q}_i) \quad (8.7)$$

$$= \sum_i e_i^2\,\sigma(e^+e^- \to \mu^+\mu^-)_{QED} \quad (8.8)$$

and hence

$$R \equiv \frac{\sigma(e^+e^- \to \text{hadrons})}{\sigma(e^+e^- \to \mu^+\mu^-)_{QED}} = \sum_i e_i^2 \quad (8.9)$$

so we expect to find this quantity <u>constant</u> in Q^2 and its magnitude measures <u>directly</u> the sum of the the squared charges of the fundamental fermion fields. Hence below charm theshold, the u.ds degrees of freedom are operative and as they come in three colours (e.g. spectroscopy) we have

$$R_{uds} = 3\left(\frac{4}{9}+\frac{1}{9}+\frac{1}{9}\right) = 2 \quad (8.10)$$

At higher Q^2 we will cross the threshold for production of charmed mesons. The first feature in the data will be the appearance of narrow vector mesons in the e^+e^- channel (identified with the ψ at 3.1 GeV and 3.7 GeV) followed by charm production threshold where R will rise and show complicated structure (around 4 GeV?). At higher Q^2 one anticipates that R will again show scaling (become constant) with value

$$R = 2 + e_{charm}^2 \quad (8.11)$$

$$\text{If } e_c = {}^2/_3 \text{ then } R \quad 3^1/3 \quad (8.12)$$

The data do indeed show scaling behaviour (fig.18). Frascati data at $\sqrt{Q^2} < 3$ GeV is unclear but not inconsistent with constant ~2 to 3 in magnitude. Better data from SPEAR below 3.5 GeV suggest R ~ 2.5 to 3 with no <u>obvious</u> structures. After the 4 GeV structures R appears to have settled down again to a value around $5\frac{1}{2}$. One unit of this is believed to be due to pair production of a new heavy lepton. Is the remaining $4\frac{1}{2}$ consistent with uds and c or are more quarks needed?

In non-abelian gauge theories with asymptotic freedom one expects the asymptotic value of R to be approached slowly from above. Hence I would regard the e^+e^- annihilation data as being a remarkable manifestation of the scaling idea and maybe even of the simple quark-parton model.

If the partons have spin $\frac{1}{2}$ we expect $\sigma_T >> \sigma_L$ at large Q^2 and the partons to be produced with a $1 + \cos^2\theta$ angular distribution (relative to the e^+e^- axis). The hadron fragments from the partons will, at high energies, be produced in a cone along the direction of motion of the parent parton. Hence we expect to see jets of hadrons with a $1 + \cos^2\theta$ distribution. This remarkably appears to be manifested by the high energy data. We will show this in section 10 but first will prepare the scene by discussing the general features of quark fragmentation into hadrons and with particular reference to the inclusive hadron production in $ep \to eh$ ..., $\nu p \to \mu h$ ... $e^+e^- \to h$ ... etc.

9. Inclusive production of hadrons and the quark-parton model.

Interesting tests of the quark-parton model arise from inclusive hadron production experiments like $e^+e^- \to h$ + anything, and $e(\nu)N \to e(\mu^-)h$ + anything. In particular the production of detected hadrons h in the current fragmentation region* of the $e(\nu)$ scattering experiments is intimately related with the production in e^+e^- annihilation, and there is some support that this correlation is in fact realised in the data.

1) $\ell N \to \ell' h \ldots . (\ell \equiv e, \mu, \nu)$

This process is illustrated in figure 18. The hadron and nucleon momenta are p_h, p_N respectively and $X \equiv Q^2/2M\nu$ as usual. There is great similarity with the ℓN inclusive process discussed earlier, but now we have an extra kinematical degree of freedom associated with p_h, the momentum of the hadron h detected. We will work in the centre of mass system of the current (γ or W) and nucleon, and will define the positive Z axis to be the γ-direction. Then we choose variables to characterise the problem:

$$Q^2,\ X(\equiv Q^2/2M\nu),\ p_T^h,\ Z(\equiv p_z^h/p_{z(max)}^h)^+ \qquad (9.1)$$

We will concentrate on the current fragmentation region ($Z > 0$). The parton model analysis of this process is illustrated in the Breit frame of the current and the parton with which it interacts (fig. 19). The nucleon carries a large longitudinal momentum P and is treated as a collection of independent pointlike constituents (partons). The current, with momentum

$$q = (0;\ 0\ 0\ -2\ x\ P) \qquad (9.2)$$

interacts incoherently with a parton whose momentum vector is

$$p = (xP;\ 0\ 0\ xP) \qquad (9.3)$$

and so its momentum is reversed. This is analogous to the total cross-section description of section 3 (fig. 6), and this part of the process is described by the quark-parton distribution functions u(x) dx etc. (the average number of u quarks in an interval dx of x) that we met in section 3-5.

In fig. 19a we exhibit the fragmentation of the quark-parton into hadrons, one of which, h, is observed.

---

*Defined later

+One often meets rapidity $\eta \equiv \tfrac{1}{2}\ell n \dfrac{E^h + p_z^h}{E^h - p_z^h}$

where E^h is the hadron's energy.

Technical Aside

There are two rather different regions, $Z \lesssim 0$. In both of these $q.p_h \sim O(Q^2)$ while $p_N.p_h$ is finite for $Z < 0$ but grows as $O(Q^2)$ for $Z > 0$. The former is intuitively the target fragmentation region and, for the reader familiar with parton model diagrams, can be represented by

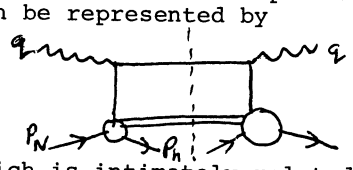

which is intimately related to the diagram met in the total cross-section at large Q

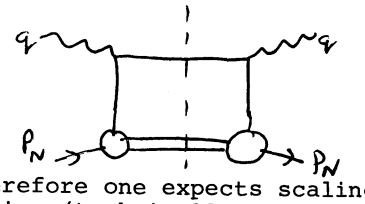

Therefore one expects scaling in this region (technically, one can argue that the light-cone dominates here).

The natural picture for $Z > 0$ is

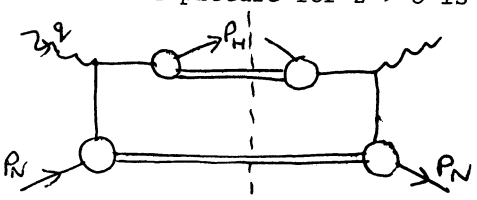

with p^h emerging along the direction of q and $p^h - q \sim O(Q^2)$. In the light-cone formalism one can say very little about this region since it is not light cone dominated (the fragmentation takes place between the two currents in the figure). Hence the parton model has extra power here if we define functions $D_i^h(Z, Q^2, p_T)$ to represent the fragmentation probabilities for (quark)-parton of flavour i to produce hadron h. See text.

The struck parton is separated by a large momentum from the nucleon fragments and so we shall assume that the fragmentation is independent of the earlier current interaction. Hence we shall assume it to be independent of and only dependent upon z, the fraction of the parton's momentum that is carried off by the observed hadron (fig. 19)

$$p^h = (zxP,\ 0,0,-zxP) \qquad (9.4)$$

and so we introduce a set of "parton fragmentation functions" $D_i^f(z)dz$ which represent the probability that parton type i produces hadron f in an interval dz about z.

2. The quark fragmentation functions

In terms of the known quark distribution functions U(X)... and the unknown $D_i^f(z)$ fragmentation functions, we can discuss hadron inclusive production in a variety of current induced processes e.g. $e^+e^- \to h..$, $ep(n) \to eh...$, $\nu p(n) \to \mu^- h...$ etc. We can obtain relations among these various processes due to the $\sum_q q(x)D_q^f(z)$ structure and constrain the relative production rates of various hadrons by limiting the number of independent $D_i^f(z)$ using isospin and charge-conjugation invariance. This yields, for π production,

$$D_u^{\pi^+} = D_d^{\pi^-} = D_{\bar{d}}^{\pi^+} = D_{\bar{u}}^{\pi^-} \qquad (9.5)$$

$$D_d^{\pi^+} = D_u^{\pi^-} = D_{\bar{u}}^{\pi^+} = D_{\bar{d}}^{\pi^-} \qquad (9.6)$$

$$D_s^{\pi^+} = D_s^{\pi^-} = D_{\bar{s}}^{\pi^+} = D_{\bar{s}}^{\pi^-} \qquad (9.7)$$

(where for simplicity we have ignored any contributions from new heavy quarks. These will in general be necessary when discussing very high energy data, but for our present introduction we will restrict our attention to data that is believed to be below threshold for production of heavy hadronic degrees of freedom such as charm).

The way these fragmentation functions enter in comparison with data depends upon the process under study. We list these below; their derivation is obvious.

i) $e^+e^- \to h...$

$$\frac{1}{\sigma_{TOT}}\frac{d\sigma}{dz}(e^+e^- \to h..) = \frac{\sum_i e_i^2 \{D_i^h(z) + D_{\bar{i}}^h(z)\}}{\sum_i e_i^2} \qquad (9.8)$$

(i = quark flavors)

(note here that the photon produces a parton-antiparton pair, either of which could have produced the observed hadron, hence the D_i and $D_{\bar{i}}$ appear, in distinction to the next examples).

ii) $ep \to eh...$

$$\frac{1}{\sigma_{TOT}}\frac{d\sigma}{dz}(ep \to eh..) = \frac{\sum_i e_i^2 f_i(x) D_i^h(z)}{\sum_i e_i^2 f_i(x)} \qquad (9.9)$$

(i = quark and antiquark flavors)

(where $f_i(x)$ are the quark-parton distribution functions of section

iii) $\nu p \to \mu^- h...$

$$\frac{1}{\sigma_{TOT}}\frac{d\sigma}{dz}(\nu p \to \mu^- h..) = \frac{d(x)D_u^h(z) + \frac{1}{3}\bar{u}(x)D_{\bar{d}}^h(z)}{d(x) + \frac{1}{3}\bar{u}(x)} \qquad (9.10)$$

(where we have approximated $\theta_c = 0$ and ignored charm).

Note that the d quark turns into a u quark before fragmenting. The 1/3 is due to the left handed current coupling to antiquarks (integration over dy having been performed as in section 6).

A. $\nu p \to \mu^- h...$

From the nature of these expressions we see that the neutrino data are a direct measurement of the fragmentation functions for pions since from eq. 9.5, 9.6

$$D_u^{\pi^\pm} \equiv D_{\bar{d}}^{\pi^\pm} \qquad (9.11)$$

and so the $d(x) + \bar{u}(x)$ cancels in numerator and denominator of eq. 9.10 yielding

$$\frac{1}{\sigma_{TOT}}\frac{d\sigma}{dz}(\nu p \to \mu^- \pi^\pm ..) = D_u^{\pi^\pm}(z) \qquad (9.12)$$

Also $\frac{1}{\sigma_{TOT}}\frac{d\sigma}{dz}(\bar{\nu} p \to \mu^+ \pi^\pm ..) = D_d^{\pi^\pm}(z) = D_u^{\pi^\mp}(z)$ (9.13)

Data from Gargamelle on the ratio of π^+/π^- production with ν/beams (and equivalently π^-/π^+ with $\bar{\nu}$) are shewn in fig. 20. These directly yield

$$\eta(z) \equiv D_u^{\pi^+}(z) \Big/ D_u^{\pi^-}(z) \qquad (9.14)$$

and we see this is of order 3 for $0.3 \leq z \leq 0.7$ rising as $z > 0.7$. That this ratio is greater than 1 is intuitively reasonable since π^+ is $u\bar{d}$ in the simplest configuration. It has been widely argued that, as $z \to 1$, $\eta(z) \to \infty$ due to the presence of u valence quark in π^+ whereas U in π^- is in the sea. Whether or not these data support this is unclear since at any finite energy, $\eta(z \to 1) \to \infty$ due to the fact that $\nu p \to \mu^-$ + (charge 2) in the quasi exclusive limit. What is of immediate interest is that

$$\eta(z)_{0.3 \leq z \leq 0.7} \simeq 2 \text{ to } 3 \qquad (9.15)$$

is consistent with the inelastic electroproduction data (discussed in a moment) and also that the data support the implication of eq. 9.12 viz

$$\frac{\frac{d\sigma}{dz}(\nu p \to \mu^- \pi^+ ..)}{\frac{d\sigma}{dz}(\nu p \to \mu^- \pi^- ..)} = \text{independent of } x \qquad (9.16)$$

The data with $0.3 < z < 0.7$ are shown as a function of x in fig. 21 and are indeed consistent with this prediction.

Very recent data from the 15' Hydrogen bubble chamber at Fermilab yield information on the production of positives and negatives separately. (fig. 22). The ratio of +/- production is qualitatively in agreement with the lower energy Gargamelle data, namely +/- > 1 and rising as z increases, though the difference between positive and negative production appears to be rather larger at Fermilab than the Gargamelle data at a comparable z. one reason may be due to the Fermi lab experiment being all positive (negative) charges whereas Gargamelle is explicitly $\pi^{\pm}$, also there may be some contamination from quasi exclusive channels that have a $Q^2(E_\nu)$ dependence that has to be taken into account before a proper comparison can be made.

If the hadrons are dominantly π and K then

$$\frac{\langle n^+\rangle}{\langle n^-\rangle} = \frac{D_u^{\pi^+}(z) + \dfrac{d(x)D_u^{K^+}(z) + \frac{1}{3}\bar{u}(x)D_{\bar{d}}^{K^+}(z)}{d(x) + \frac{1}{3}\bar{u}(x)}}{D_u^{\pi^-}(z) + \dfrac{d(x)D_u^{K^-}(z) + \frac{1}{3}\bar{u}(x)D_{\bar{d}}^{K^-}(z)}{d(x) + \frac{1}{3}\bar{u}(x)}} \qquad (9.17)$$

The contribution from antiquarks is believed to be very small (section so let's neglect them for simplicity so that we have

$$\frac{\langle n^+\rangle}{\langle n^-\rangle} = \frac{D_u^{\pi^+}(z) + D_u^{K^+}(z)}{D_u^{\pi^-}(z) + D_u^{K^-}(z)} \qquad (9.18)$$

Hence

$$\frac{\langle n^+\rangle}{\langle n^-\rangle} > \frac{\langle n^{\pi^+}\rangle}{\langle n^{\pi^-}\rangle} \quad \text{if} \quad \frac{D_u^{K^+}}{D_u^{K^-}} > \frac{D_u^{\pi^+}}{D_u^{\pi^-}} \qquad (9.19)$$

B. ep(n) → eh...

The analysis of inelastic electron scattering is slightly more involved than for neutrinos due to the contributions from all the charged quarks:

$$\frac{1}{\sigma_{TOT}}\frac{d\sigma}{dz}(eN \to eh..) = \frac{\sum_i e_i^2 f_i(x) D_i^h(z)}{\sum_i e_i^2 f_i(x)} \qquad (9.20)$$

For ease of notation I shall normalise to the total cross section (W_1) and write

$$N_i^h(x,z) = \sum_i e_i^2 f_i(x) D_i^h(z) \qquad (9.21)$$

(this quantity is $L_i^h(x2)$ in Feynmans book ref. F1)

In their original analysis of the data of Bebek et al ($Q^2 = 2$ GeV^2, $\omega = 4$) Cleymans and Rodenberg (CR) ignored the contribution from all but the valence quarks which is reasonable for $\omega \simeq 4$. Hence in $ep \to e\pi^{\pm}...$ they have (writing $u(x) \equiv f_u(x)$ etc.)

$$\frac{N^{\pi^+}(x,z)}{N^{\pi^-}(x,z)} = \frac{\frac{4}{9}u(x)D_u^{\pi^+}(z) + \frac{1}{9}d(x)D_d^{\pi^+}(z)}{\frac{4}{9}u(x)D_u^{\pi^-}(z) + \frac{1}{9}d(x)D_d^{\pi^-}(z)} \qquad (9.22)$$

$$= \frac{4u(x)\eta(z) + d(x)}{4u(x) + d(x)\eta(z)} \qquad (9.23)$$

where in the final step we utilised the relations eq. 9.5-9.7 and, as before, defined

$$\eta(z) \equiv D_u^{\pi^+}(z) \Big/ D_u^{\pi^-}(z) \qquad (9.24)$$

The Bebek data are consistent with scaling in the range $0.2 \leq z \leq 0.7$ and so the analysis was limited to this region for which $\langle n^{\pi^+}\rangle/\langle n_{\pi^-}\rangle \simeq 2$ independent of z. For $\omega \simeq 4$ approximately $u(x) = 2d(x)$ and so

$$2 \simeq \frac{8\eta(z) + 1}{8 + \eta(z)} \qquad (9.24)$$

which yields $\eta(z) \simeq 2.5$ $0.2 \leq z \leq 0.7$. This is in perfect agreement with the Gargamelle data on $\pi^{\pm}$ production by neutrino beams (eq. 9.15) and so we have strong support here for the quark-parton picture of the semi-inclusive hadron production.

Dakin and Feldman (DF) refined and extended the above analysis by incorporating later data in the range $0.5 < Q^2 < 2.5$ GeV^2 and $3 \leq \omega \leq 60$ and allowing for the contribution of valence and sea quarks. They parametrised the longitudinal momentum distributions of the quarks as follows

$$\begin{aligned} u(x) &= u_v(x) + K(x) \\ d(x) &= d_v(x) + K(x) \\ s(x) &= \bar{s}(x) = \bar{u}(x) = \bar{d}(x) = K(x) \end{aligned} \qquad (9.25)$$

where $u_v(x)$, $d_v(x)$ represent the distribution functions for valence quarks and the sea was hypothesised to be SU(3) symmetric (this is not a very crucial assumption for their analysis it turns out).

These functions u(x), K(x) etc. were taken from the McElheney and Tuan fits to the total cross-section data (this is essentially the Kuti Weisskopf model modified to take account of the fact that

$\nu W_2^{en}/\nu W_2^{ep} < 2/3$ as $x \to 1$).

Then one has, in place of eq. 9.23

$$\frac{N^{\pi^+}(x,z)}{N^{\pi^-}(x,z)} = \frac{4u_v(x)\eta(z)+d_v(x)+(S\eta(z)+7)K(x)}{4u_v(x)+\eta(z)d_v(x)+(S\eta(z)+7)K(x)} \qquad (9.26)$$

The Cleymans-Rodenberg formula, eq. 9.23, is obtained when $K(x) \to 0$ (and hence $u_v \equiv u$ etc.). The effect is to raise $\eta(z)$ slightly as compared to $K(x) = 0$:

$$\eta(z) \simeq 3.0 \pm 0.6 \qquad (9.27)$$

(compare $\eta(z) \simeq 2.5$ when $K(x) = 0$ as in Cleymans-Rodenberg). Qualitatively it is obvious that this should be so since the sea populates π^+ and π^- equally, hence tends to dilute the ratio. To have the same ratio as in the data then $\eta(z)$ must be larger than in the analysis where the sea was ignored.

Having determined $\eta(z)$ and knowing the $f_i(x)$ from the McElhaney-Tuan parametrisation of the total cross-section data then one can predict the $x(\omega)$ dependence of the π^+/π^- production ratio using eq. 9.26. This quantity is compared with the data in fig. 23.

Due to the dominance of $u(x)$ as $x \to 1$, more positive charge is predicted to be forward produced.

The production from neutron targets is immediately obtained by interchanging U_v and d_v in eq. 9.26 while $K(x)$ is the same as before (the sea has $I = 0$)

Hence

$$\left[\frac{N^{\pi^+}}{N^{\pi^-}}(x,z)\right]^{en} = \frac{4d_v(x)\eta(z)+u_v(x)+(S\eta(z)+7)K(x)}{4d_v(x)+\eta(z)u_v(x)+(S\eta(z)+7)K(x)} \qquad (9.28)$$

So that with $\eta(z) \simeq 3$ we immediately predict the curve of fig. 23 which is compared with the data

Note the general feature that as $\omega \to \infty$ ($x \to 0$) the π^+/π^- ratio tends to unity (sea dominance). Coming to smaller ω the ratio rises and then as $\omega \to 1$ falls below 1 due to dominance of the U_T quark. In general with U quark dominance

$$\frac{\pi^+}{\pi^-}(x \to 1) \longrightarrow \frac{1}{\eta} \text{ in en} \qquad (9.29)$$

$$\longrightarrow \eta \text{ in ep} \qquad (9.30)$$

Footnote A cautionary note is provided by Hanson at the Stanford Symposium. Plotting the π^+/π^- ratios against x and also W for various Q^2 (N the mass of hadronic system) one cannot yet tell if i) π^+/π^- is a function only of ω i.e. scales in $\omega(x)$ or ii) function only of W. The variation of π^+/π^- with W or x over the measured range of parameters is too small to see a significant difference between the two.

Further oritentation on the significance of these production ratios is obtained by noting that in the photon fragmentation region at $Q^2 = 0$ $\pi^+/\pi^- = 0.8$ This is quite different from the values 1.2 to 1.3 predicted at moderate ω in the present model for $Q^2 \neq 0$.

Sum Rules in eN → eh...

Normalising to $F_1^{eN}(x)$, the number of hadrons i in the current fragmentation region, with momentum z in an experiment done at fixed x reads

$$N^i(z,x) = \frac{4}{9}\left(u(x)D_u^i(z) + \bar{u}(x)D_{\bar{u}}^i(z)\right) + \frac{1}{9}\left(d(x)D_d^i(z) + \bar{d}(x)D_{\bar{d}}^i(z)\right) + \frac{1}{9}\left(s(x)D_s^i(z) + \bar{s}(x)D_{\bar{s}}^i(z)\right) \qquad (9.31)$$

plus further possible contributions from charmed quarks etc. We can simplify this messy expression by studying, for example, the excess of π^+ over π^-

$$N^{\pi^+}(z,x) - N^{\pi^-}(z,x) = \left[D_u^{\pi^+}(z) - D_u^{\pi^-}(z)\right]\left[\frac{4}{9}(u-\bar{u}) - \frac{1}{9}(d-\bar{d})\right](x) \qquad (9.32)$$

where we used relations like $D_s^{\pi^+} = D_s^{\pi^-}$ etc. (eq. 9.7). (This expression is true in general since further quarks with $I = 0$ will not contribute to the $\pi^+\pi^-$ difference).

Since we know from the proton a neutron charge sum rules (eq. 4.24-4.26)

$$\int[u(x) - \bar{u}(x)]\,dx = 2\int[d(x) - \bar{d}(x)]\,dx = 2 \qquad (9.33)$$

then

$$\int dx\,(N_{ep}^{\pi^+} - N_{ep}^{\pi^-})(z,x) = \left[D_u^{\pi^+}(z) - D_u^{\pi^-}(z)\right]\frac{7}{9} \qquad (9.34)$$

Similarly on neutron targets one derives (interchanging u, d in eq. 9.32)

$$N_{en}^{\pi^+}(z,x) - N_{en}^{\pi^-}(z,x) = \left[D_u^{\pi^+}(z) - D_u^{\pi^-}(z)\right]\left(\frac{4}{9}(d-\bar{d}) - \frac{1}{9}(u-\bar{u})\right)(x) \qquad (9.35)$$

and so

$$\int_0^1 dx\,(N_{en}^{\pi^+} - N_{en}^{\pi^-})(z,x) = \left[D_u^{\pi^+}(z) - D_u^{\pi^-}(z)\right]\frac{2}{9} \qquad (9.36)$$

Consequently, independent of z or $P_{n,t}^2$,

$$\frac{\int dx\,(N^{\pi^+}(z,x) - N^{\pi^-}(z,x))^{en}}{\int dx\,(N^{\pi^+}(z,x) - N^{\pi^-}(z,x))^{ep}} = \frac{2}{7} \qquad (9.37)$$

Experimentally it is more useful to integrate over all z and since

$$\frac{\int dz\, N_{en}^{\pi^+}(z,x)}{\int dz\, N_{ep}^{\pi^+}(z)} \equiv \frac{\int dz \left(\frac{d\sigma}{dz}\right)_{en}^{\pi^+}}{\int dz \left(\frac{d\sigma}{dz}\right)_{ep}^{\pi^+}} \qquad (9.38)$$

then

$$\frac{\int_0^1 dx\, F_1^{en}(x)\left(\langle n_{\pi^+}\rangle_{en} - \langle n_{\pi^-}\rangle_{en}\right)}{\int_0^1 dx\, F_1^{ep}(x)\left(\langle n_{\pi^+}\rangle_{ep} - \langle n_{\pi^-}\rangle_{ep}\right)} = \frac{2}{7} \qquad (9.39)$$

where $\langle n_i \rangle$ is the average multiplicity of particle i as a function of x. This sum rule was derived by Gronau et al. but is not yet well tested by data.

C. $e^+e^- \to h\ldots$

In equation 9.8 we have

$$\frac{1}{\sigma_{TOT}}\frac{d\sigma}{dz}(e^+e^- \to h\ldots) = \frac{\sum_i e_i^2 \{D_i^h(z) + D_{\bar{i}}^h(z)\}}{\sum_i e_i^2} \qquad (9.40)$$

or, since*

$$\sigma_{TOT}/\sigma_{\mu\mu} \equiv R = 3\sum_i e_i^2 \quad \text{then}$$

$$\frac{1}{\sigma_{\mu\mu}}\frac{d\sigma}{dz}(e^+e^- \to h\ldots) = 3\sum_i e_i^2 \{D_i^h(z) + D_{\bar{i}}^h(z)\} \qquad (9.41)$$

If for small z $D(z) \sim 1/z$ (e.g. by analogy with the $f(x) \sim 1/x$ for the probability of finding given quarks in the hadron) then a logarithmic rise in multiplicity is predicted since on integrating over z

$$R\langle n_h \rangle = \int_{2m_{\mu}/\sqrt{Q^2}}^1 \frac{1}{\sigma_{\mu\mu}}\frac{d\sigma}{dz}dz = 3\sum_i e_i^2 \int_{\frac{2m}{\sqrt{Q^2}}}^1 [D_i^h + D_{\bar{i}}^h]\,dz \qquad (9.42)$$

and the lower limit on the z integral generates the logarithmic growth in Q^2. We have already seen (fig. 22) some evidence that $D(z) \sim 1/z$ as $z \to 0$ and so it is interesting to find that there may be a logarithmic growth of the multiplicity in $e^+e^- \to h\ldots$ (fig. 24).

Since $\sigma_{\mu\mu} = \frac{4\pi\alpha^2}{3s}$ then we can rewrite eq. 9.41 to read

$$s\frac{d\sigma}{dz}(e^+e^- \to h\ldots) = \frac{4\pi\alpha^2}{s} 3\sum_i e_i^2 \{D_i^h(z) + D_{\bar{i}}^h(z)\} \qquad (9.43)$$

$$\simeq 88 \times 3 \sum_i e_i^2 \{D_i^h(z) + D_{\bar{i}}^h(z)\}\ \text{nb-GeV}^2$$

*Footnote: The factor 3 is for three colours of quarks.

The distributions in $s\frac{d\sigma}{dz}$ are shown in fig. 25 and do show the possibility of scaling for $z > 0.5$. We dont expect scaling for all s here because R is rising as one passes through this complicated region. It does, however, appear that the data scale for all s when $z \geq 0.5$. This, and the z, s dependence of the scaling violation are nicely seen in fig. 2 which plots $sd\sigma/dz$ versus $E_{c.m.}$ for various z intervals. Scaling would imply that $s\frac{d\sigma}{dz}$ should be independent of $E_{c.m.}$ for any fixed z.

If the entire rise in R is due to pair production of new particles $e^+e^- \to U^+U^-$ which decay immediately into the observed hadrons then the final decay products at threshold should be limited to $z < 0.5$ since each new U is carrying half the energy. If each of these then decays, clearly half the momentum of any single decay product cannot exceed ½ of the total energy and hence $z < 0.5$. For U production slightly above threshold a few decay products can have $z > 0.5$ but their effect will be negligible so the argument holds true.

Bearing this is mind, look again at the figure 26. For $z > 0.5$ we see scaling (independence of $s\frac{d\sigma}{dz}$) for the full range of $3 \leq E_{c.m.} \leq 8$ GeV. For $z < 0.5$ the data have rescaled above 4 GeV except at the smallest values of z. Here the finite energy means that we are still seeing threshold effects and so we dont expect scaling to set in until PEP/PETRA energies. Hence, semi-quantitatively we can understand the observed behaviour as a combination of threshold and scaling phenomena.

Consequently we may suppose that the $s\frac{d\sigma}{dz}$ distribution is a superposition of "old" and "new".

If this is indeed true, then the data at 3 GeV is due entirely to "old" physics and moreover is exhibiting (for $z \geq 0.2$) the scaling behaviour of the uds quark degrees of freedom. Hence we might analyse this data in terms of the relation

$$\frac{1}{\sigma_{\mu\mu}}\frac{d\sigma}{dz}(e^+e^- \to h\ldots) = 3\sum_{i=uds} e_i^2 \{D_i^h(z) + D_{\bar{i}}^h(z)\} \qquad (9.41)$$

and compare with the analogous data on inclusive hadron production in lepto-induced reactions as discussed previously.

As orientation and to simplify matters let us just make the approximation that only the u quark is important (it is the most probable quark in the proton and also has the biggest squared charge by a factor of four). Then for ep → eh...

$$\frac{1}{\sigma_{TOT}}\frac{d\sigma}{dz} = \sum_i e_i^2 f_i(x) D_i^h(z) \Big/ \sum_i e_i^2 f_i(x) \longrightarrow D_u^h(z) \qquad (9.44)$$

and hence

$$\frac{1}{\sigma_{tot}}\left[\frac{d\sigma}{dz}(ep\to eh^+..) + \frac{d\sigma}{dz}(ep\to eh^-..)\right] \simeq D_u^{h^+}(z) + D_u^{h^-}(z) \qquad (9.45)$$

For e^+e^- annihilation at $\sqrt{Q^2} \lesssim 3.5$ GeV (where by hypothesis only the uds degrees of freedom contributes), taking $u\bar{u}$ as the largest contributor to R then

$$\frac{1}{2\sigma_T}\left[\frac{d\sigma}{dz}(e^+e^-\to h^+..) + \frac{d\sigma}{dz}(e^+e^-\to h^-..)\right] \qquad (9.46)$$

$$\simeq \frac{1}{2}\left[D_u^{h^+}(z) + D_u^{h^-}(z) + D_{\bar{u}}^{h^+}(z) + D_{\bar{u}}^{h^-}(z)\right] = D_u^{h^+}(z) + D_u^{h^-}(z)$$

and so finally one has the immediate comparison

$$\frac{1}{\sigma_T}\left(\frac{d\sigma}{dz}\right)(ep\to eh^\pm..) = \frac{1}{2\sigma_T}\left(\frac{d\sigma}{dz}\right)(e^+e^-\to h^\pm..) \qquad (9.47)$$

This comparison is shown in fig. 27 and agreement is excellent at large z where different choices for the comparison variable are less important.*

Ultimately it will be nice to see if π, K, p production separately satisfy this relation since at present $h^\pm$ means <u>all</u> hadrons of the relevant charge. Also one will attempt to separate each quark's individual contribution using ν and e data; one might already think of doing this using the data in figs. ignoring any q^2 dependence and assuming that only uds quarks are important. Then as one crosses charm (?) threshold and rescaling is seen (?) the role of the c quark fragmentation can be examined. This is in principle a straightforward extension of the present discussion which should provide enough material for the interested reader to perform the exercise for her or himself.

10. <u>Angular distributions of hadrons in $e^+e^- \to$ h anything</u>

The stored $e^\pm$ beams circulate in a magnetic field whose direction ($\hat{y}$) is perpendicular to the plane ($x\hat{z}$) of the storage ring. After a period of time the positrons (electrons) tend to populate the state where their spins are parallel (antiparallel) to the guide magnetic field, this state having lower energy than the opposite spin orientation. Consequently the storage ring beams are polarised in the $\hat{y}$ direction. If the polarisation is 100% then the photon created by the e^+e^- annihilation has zero helicity along the $\hat{y}$ direction,

$$J_y^\gamma = 0 \qquad (10.1)$$

we will calculate the angular distribution of a hadron h produced by such a polarised photon in

$$e^+e^- \to \gamma \to h + \text{anything}$$

If the hadron emerges at angle θ relative to the $\hat{z}$ axis (the e^+ direction) and ϕ relative to the $x\hat{z}$ plane of the ring then the direction of its momentum vector is

$$\hat{p}_h = (\sin\theta\cos\phi,\ \sin\theta\sin\phi,\ \cos\theta) \qquad (10.2)$$

illustrated in the figure 28, so that the angle β between the hadron momentum vector and the $\hat{y}$ axis is given by

$$\cos\beta = \sin\theta\sin\phi \qquad (10.3)$$

The expression for the angle β enables us to immediately calculate

$$\frac{d\sigma}{d\Omega}(e^+e^-\to h..)$$

If λ = helicity of the photon along h (i.e. spin projection along $\hat{p}_h$)

then since

β = angle between $\hat{p}_h$ and $\hat{y}$

and

photon spin projection = 0 along $\hat{y}$

we have

$$\left(\frac{d\sigma}{d\Omega}\right) \propto \sum_{\lambda=\pm1,0} |A_\lambda|^2 \left|d^1_{\lambda 0}(\beta)\right|^2 \qquad (10.4)$$

($d^1_{MM'}$ because J = 1 for e^+e^- annihilation through a single photon). Parity forces

$$|A_1| = |A_{-1}| \qquad (10.5)$$

and so

$$\left(\frac{d\sigma}{d\Omega}\right) \propto |A_1|^2\sin^2\beta + |A_0|^2\cos^2\beta \qquad (10.6)$$

*<u>Footnote</u>: Gilman[2] here used $X_{c.m.}$ for ep → eh.. and $x = \frac{2p}{\sqrt{Q^2}}$ for e^+e^- → h.. As $Q^2 \to \infty$, $X, X_{c.m.} \to z$. At present energies the choice of variables can make a significant difference at small z but differences are less important at large z since all particles are relativistic there.

We define the transverse and longitudinal cross-sections proportional to $|A_1|^2$ and $|A_0|^2$ respectively, and these are functions of Q^2 (the photon squared mass) and p_h (the momentum of the produced hadron)*. These functional dependences are implicit in all the following equations. We can therefore write

$$\left(\frac{d\sigma}{d\Omega}\right)_{pol.} = \sigma_T \sin^2\beta + \sigma_L \cos^2\beta = \sigma_T + (\sigma_L - \sigma_T)\sin^2\theta\sin^2\phi \qquad (10.7)$$

The subscript "pol." is to remind us that this is the cross-section arising from a completely polarised photon (e^+e^- beams). If instead we had unpolarised beams then

$$\left(\frac{d\sigma}{d\Omega}\right)_{unpol} = \sigma_T + (\sigma_L - \sigma_T)\sin^2\theta \cdot \frac{1}{2} \qquad (10.8)$$

since $\langle\sin^2\phi\rangle = \frac{1}{2}$. Consequently in general, for a degree of polarisation P

$$\left(\frac{d\sigma}{d\Omega}\right) = (1-P^2)\left(\frac{d\sigma}{d\Omega}\right)_{unpol.} + P^2\left(\frac{d\sigma}{d\Omega}\right)_{pol.} \qquad (10.9)$$

and so

$$\left(\frac{d\sigma}{d\Omega}\right) = \frac{1}{2}(\sigma_T + \sigma_L)\left[1 + \alpha\left(\cos^2\theta + P^2\sin^2\theta\cos 2\phi\right)\right] \qquad (10.10)$$

with

$$\alpha \equiv \frac{\sigma_T - \sigma_L}{\sigma_T + \sigma_L} \qquad (10.11)$$

Equation 10.10 is the general angular distribution for the inclusive hadron production in electron positron annihilation through one photon. From the observed angular distributions of h one can determine $\sigma_L/\sigma_T(z,Q^2)$ which contains the interesting dynamical information (in the model where the hadrons are the fragmentation products of spin ½ partons then $\sigma_L/\sigma_T \sim 1/Q^2$).

In <u>principle</u> one can determine σ_L/σ_T, or equivalently α, from the θ distribution alone and so the polarisation P gives no additional information. In <u>practice</u> since the SPEAR detector has rather limited acceptance in θ, $|\cos\theta| \leq 0.6$, (due to the open ends of the cylindrical detector which allow the beams to enter and depart) while there is complete acceptance in ϕ, then it is easier to separate σ_L/σ_T from the ϕ dependence, i.e. exploiting the polarised beams. This is illustrated clearly in the data (Schwitters, Stanford Conference 1975). Integrating over ϕ one has

$$\frac{d\sigma}{d\Omega} = \frac{1}{2}(\sigma_T + \sigma_L)(1 + \alpha\cos^2\theta) \qquad (10.12)$$

*<u>Footnote</u>: More usually chosen as Q^2 and $z = 2P/\sqrt{Q^2}$, see section 9.

and the θ distributions very poorly determine α (fig. 29).

The inclusive azimuthal distributions for particles with $z > 0.3$ and $|\cos\theta| \leq 0.6$ are exhibited in figs. 27 for two energies 7.4 GeV and 6.2 GeV in the c.m. There is a very clear $\cos 2\phi$ dependence in the data sample taken at $E_{c.m.} = 7.4$ GeV. At 6.2 GeV there happens to be a depolarising resonance in the SPEAR ring (a matching of the machine parameters and the g_e-2 such that the spins of $e^\pm$ process by an exact integer number of turns per orbit). Hence at 6.2 GeV the beams are "accidentally" unpolarised and an isotropic ϕ distribution emerges.

Using the $E_{c.m.} = 7.4$ GeV data with its clear $\cos 2\phi$ dependence we can determine α by making a best fit to the form of $d\sigma/d\Omega$ (eq. 10.10) once we have obtained the magnitude of ρ^2. This quantity is found by fitting the distributions for $e^+e^- \to \mu^+\mu^-$ data which are collected at the same time as the hadronic production data and as $(\sigma_L/\sigma_T)_{\mu^+\mu^-} \simeq 0$ then

$$\left(\frac{d\sigma}{d\Omega}\right)_{e^+e^- \to \mu^+\mu^-} = \frac{1}{2}\sigma_T\left(1 + \cos^2\theta + P^2\sin^2\theta\cos 2\phi\right) \qquad (10.13)$$

Hence P^2 is determined and found to be 0.46 ± 0.05 at this energy. One now uses this information in fitting the hadronic sample and α (or σ_L/σ_T) is obtained for $e^+e^- \to h$...

The results for σ_L/σ_T (and α) as functions of z at $E_{c.m.} = 7.4$ GeV are shown in fig. 30. At low z where the hadron h is recoiling against a high mass system near to threshold (it is produced nearly at rest) σ_L and σ_T are almost equiprobable. At $z \gtrsim 0.2$, where Bjorken scaling was observed (section 9), σ_T dominates, characteristic of production of pairs of spin ½ particles (c.f. $\mu^+\mu^-$).

Hence the data are consistent with the model where the observed hadrons are emitted by spin ½ partons.

Further support for the idea that the hadrons are parton fragments comes from a study of the multiprong hadronic events, where it is found that these have a "jet" structure (limited momentum transverse to some axis). This phenomenon is familiar in hadron physics and is a natural consequence of the parton model. The picture is that at high $E_{c.m.}$ the spin ½ partons are produced with angular distribution typical of $\alpha = 1$ and that the final state observed hadrons will limit momenta transverse to the direction θ in which the partons were produced. Hence two jets of particles will be expected, the jet axis being the memory of the original parton direction.

In those events with ≥ 3 hadrons a search was made for an axis which minimised the sum of the squares of the momenta perpendicular to it. For any event, having found this axis, then a quantity S called the "sphericity" is defined.

$$S = 3\sum_i p_{T_i}^2 \Big/ 2\sum_i p_i^2 \; ; \; 0 \le S \le 1 \qquad (10.14)$$

where p_i, p_{T_i} are the i-th particle's momenta and its momenta transverse to the jet axis. Events with $S \to 0$ are jetlike while $S \to 1$ are spherical. The sphericity distributions at three different energies are shown in fig.I9 of Scwitter's talk on page 20 of the Stanford conference. The mean sphericity plotted versus $E_{c.m.}$ is shown in fig31 and as the energy increases the increasingly jetlike character of the events is apparent.

While much work still remains to be done here these effects do appear to b e more than j ust correlations arisisng from energy-momentum conservation and are genuine multiparticle effects. A comparison with a Monte Carlo jet model with $\langle p_T \rangle \simeq 350 \text{MeV}/c$ is an excellent description of the data whereas the Monte Carlo phase space model is poor. The inclusive angular distribution is also well fitted by the jet model and for $E_{c.m} = 7.4\text{GeV}$ the display is shown in fig32 with

$$\alpha_{jet} = 0.78 \pm 0.12$$

The momenta of the hadrons relative to the jet produce the range of values in the shaded part of the figure.

BIBLIOGRAPHY

FI. R.P.Feynman "Ph oton-Hadron interactions (Benjamin,N.Y. I972)

Proceedings of the Stanford Conference I975 In particular the talks by Gilman,Harari, Scwitters,Llewellyn Smith and as cited in the list by chapters below.

C.H.Llewellyn Smith,Physics Repts3C,264(72)

P.Landshoff,CERN-Rept-74-22,(I974 Summer School in this series)

J.Kuti and V.Weisskopf,Phys RevD4,34I8(7I)
P.Landshoff and J.Polkinghorne,Nucl.Phys B28,240(7I)

Chapter 6-7

HPWF collaboration:Gargamelle collaboration I5'bubble chamber : pp5II-57I of Stanford Conference,op cit

Inelastic electron and muon scattering: L.Mo and also R.Taylor in P65I-670 of Stanford conference op cit.

CSS: F.E.Close,D.M.Scott and D.Sivers, Phys.Letters62B,2I3(76)

Chapter9

J.Cleymans and R.Rodenberg,Phys RevD9,I55(74)
J.Dakin and G.Feldman,Phys.RevD8,2862(73)

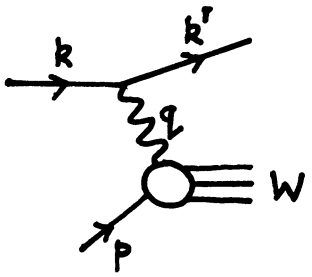

Fig. 1 Inelastic electron scattering

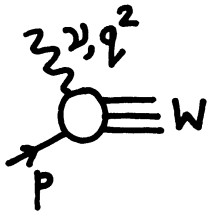

Fig. 2 Virtual photoabsorption

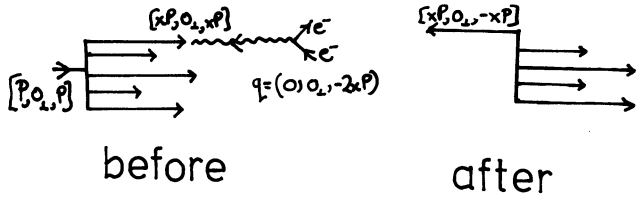

Fig. 6 Current-nucleon scattering in the current-parton Breit frame

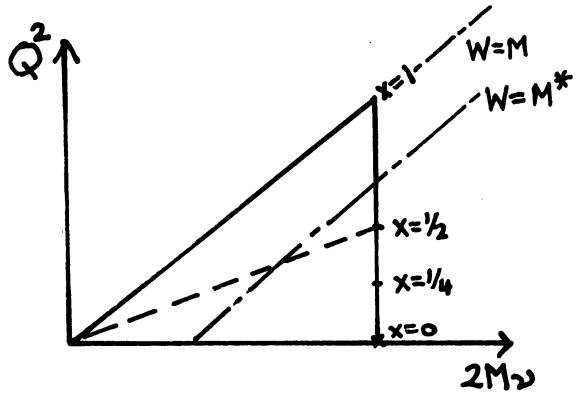

Fig. 3 ν, Q^2 kinematic region

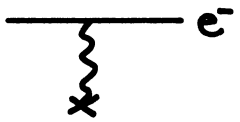

Fig. 7 Electron scattering in a Coulomb field

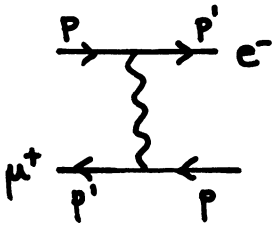

Fig. 8 Electron-muon scattering

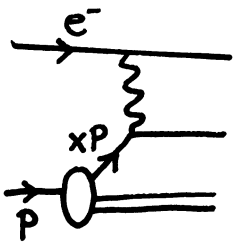

Fig. 9 Electron-parton scattering

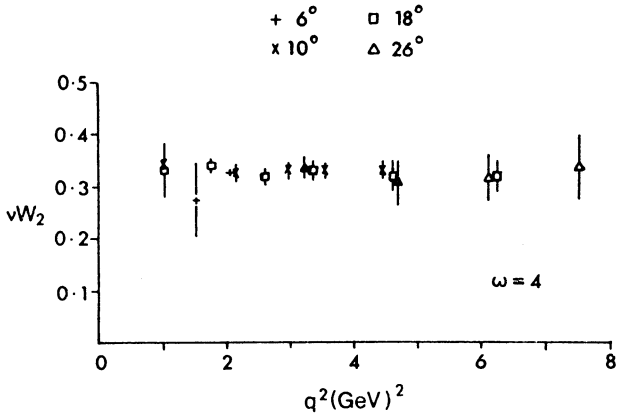

Fig. 4 $\nu W_2(\omega=4)$-Q^2 independence

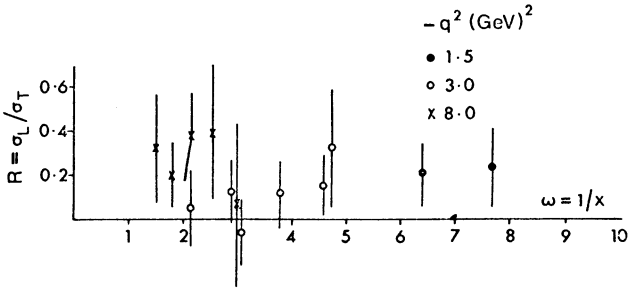

Fig. 5 $R(\sigma_L/\sigma_T)$

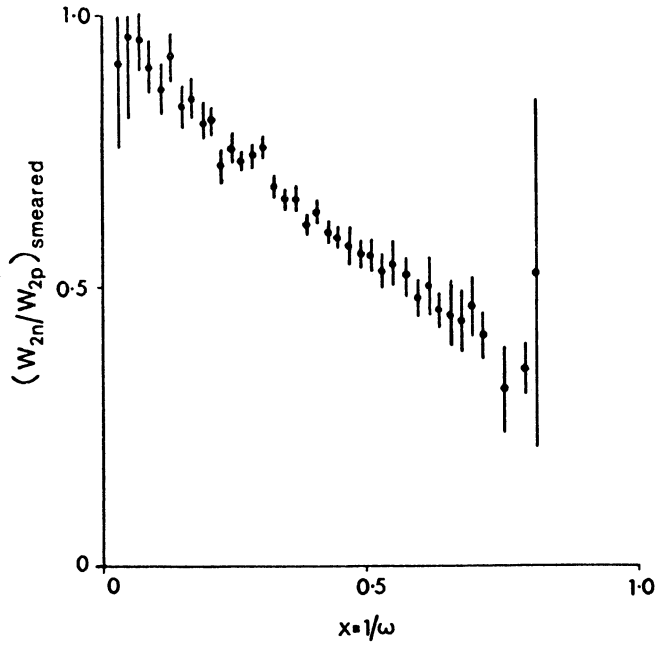

Fig. 10 Neutron to proton structure function ratio for electron scattering

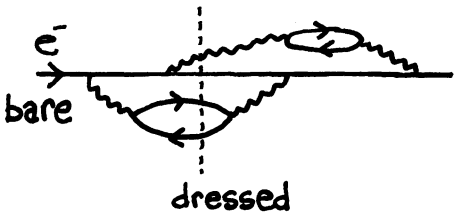

Fig. 11 Dressing a bare electron in QED

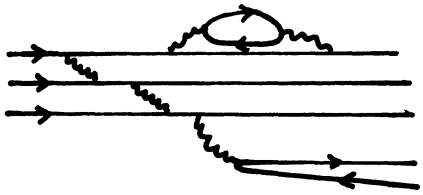

Fig. 12 Dressing a bare quark with gluons

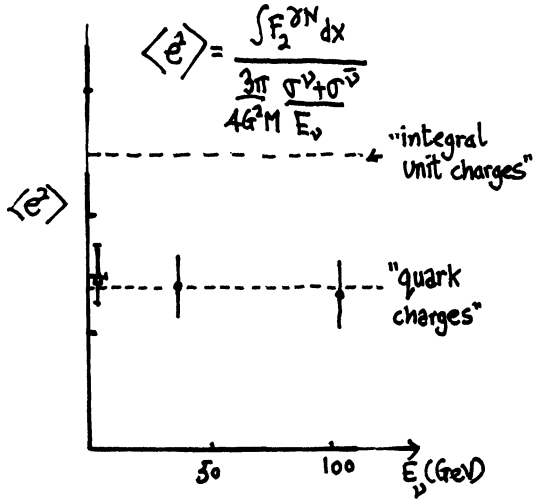

Fig. 13 CERN-GGM data comparing inelastic neutrino and SLAC data

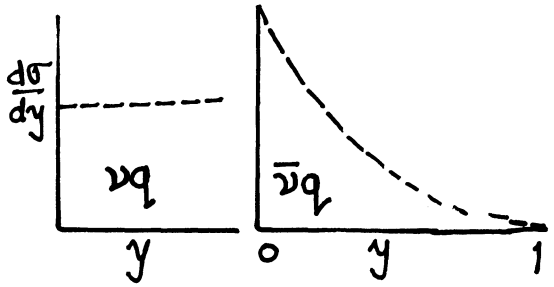

Fig. 14 y dependence of neutrino-quark and antiquark scattering

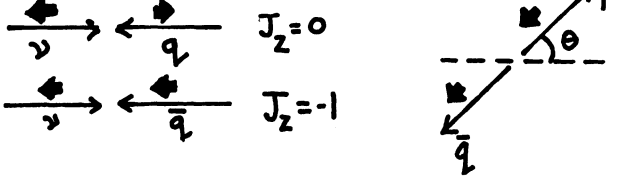

Fig. 15 Neutrino-quark and antiquark angular distributions

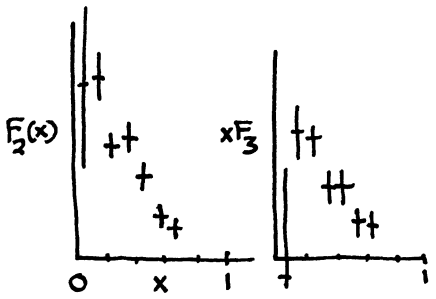

Fig. 16 F_2 and xF_3 from Gargamelle

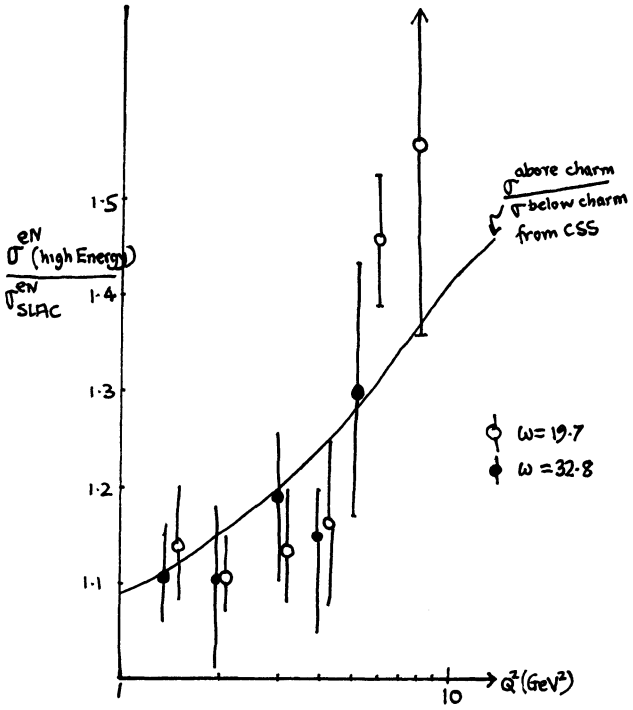

Fig. 17 Violation of scaling in inelastic muon scattering above charm production threshold and comparison with data from the Chen-Hand experiment (from CSS)

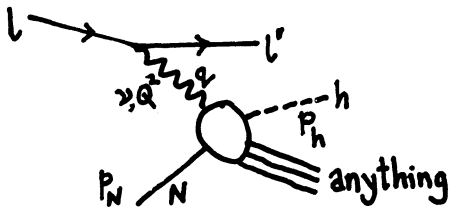

Fig. 18 Inclusive hadron production in the parton model

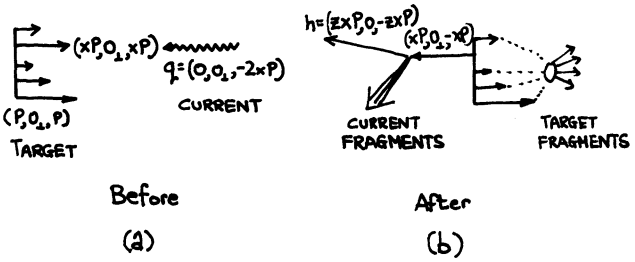

Fig. 19 Quark fragmentation into hadrons

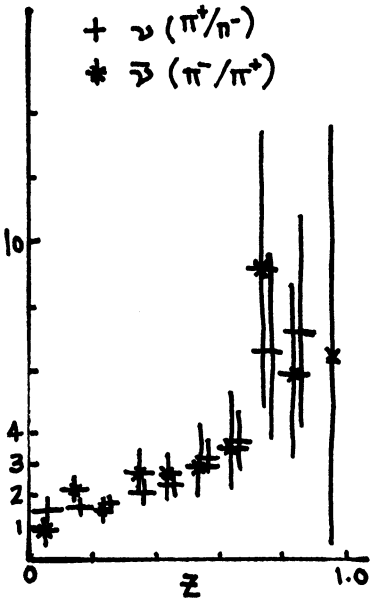

Fig. 20 Gargamelle data on pion production by neutrino and antineutrino beams

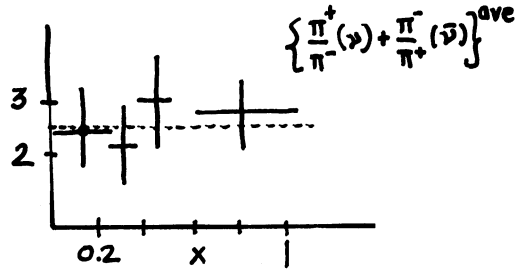

Fig. 21 x independence of pion production in neutrino experiments (π^+/π^- ratio) for $0.3 \leq z \leq 0.7$

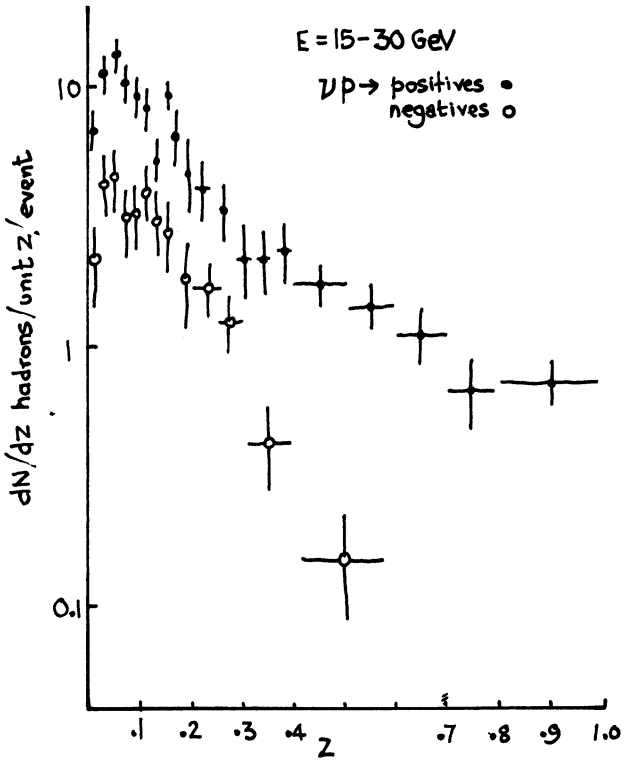

Fig. 22 Positive and negative hadron production by neutrinos in the Fermilab 15' bubble chamber

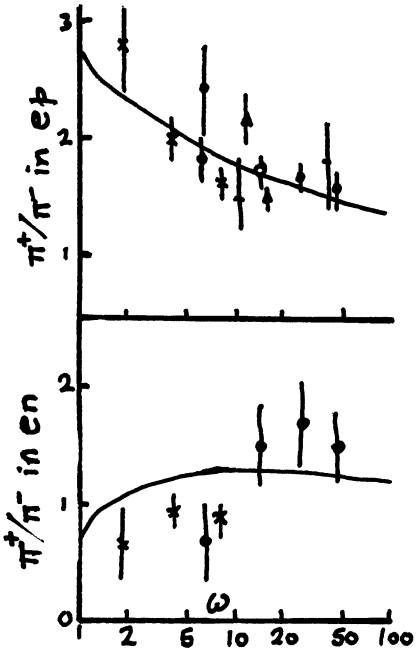

Fig. 23 ep, en → π^+/π^-

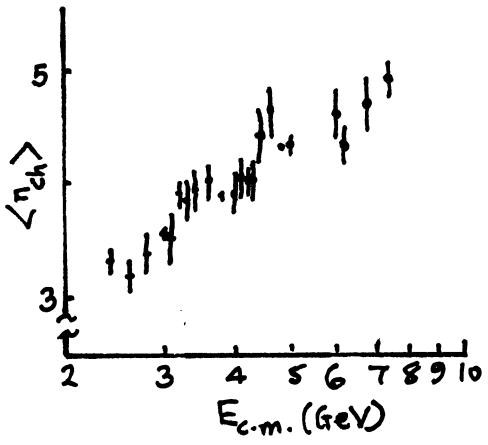

Fig. 24 Logarithmic growth in hadron multiplicity in e^+e^- annihilation

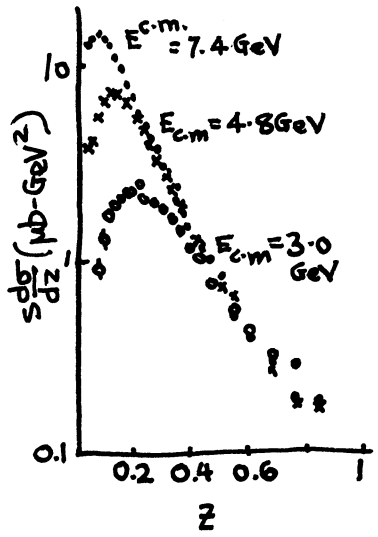

Fig. 25 s(dσ/dz) for e^+e^- → h ...

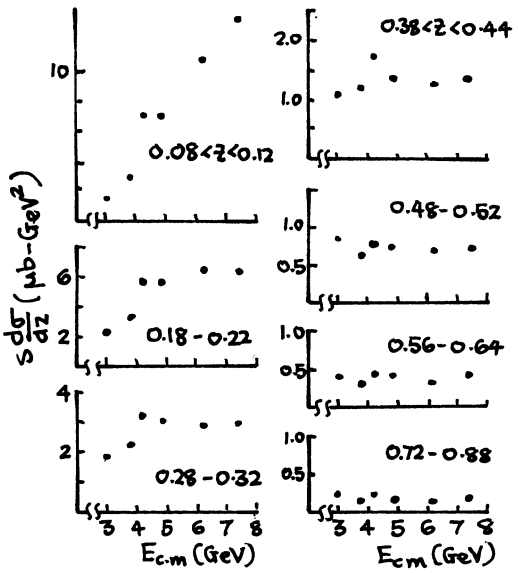

Fig. 26 As fig. 25, plotted against $E_{c.m.}$

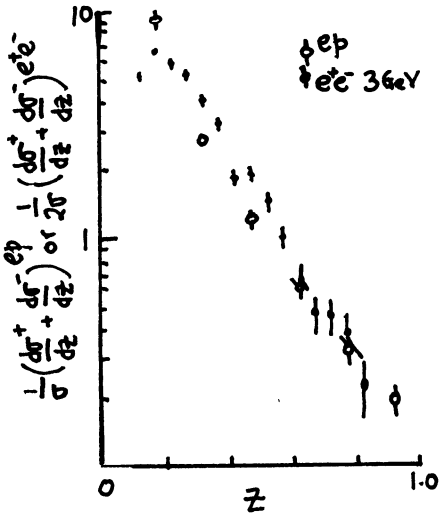

Fig. 27 Comparison of hadron production in ep and $e^+e^- \to h$ ...

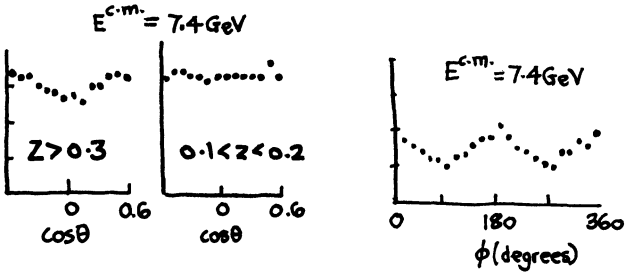

Fig. 29 Angular distribution of $e^+e^- \to h$ ...

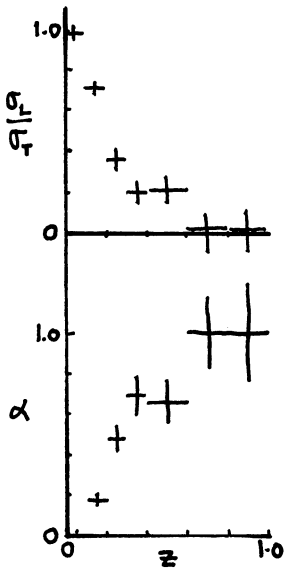

Fig. 30 (σ_L/σ_T) and α at 7.4 GeV

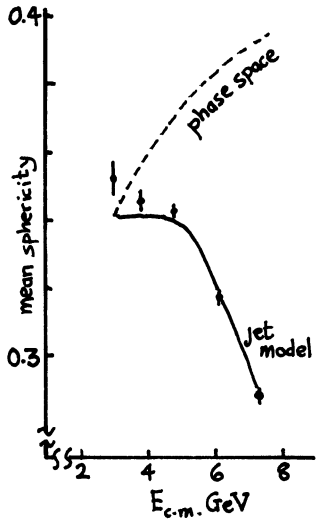

Fig. 31 Mean sphericity versus $E_{c.m.}$

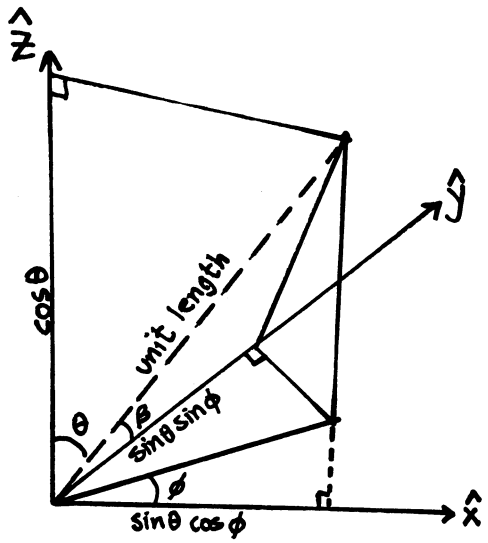

Fig. 28 $\hat{p}_h$ vector

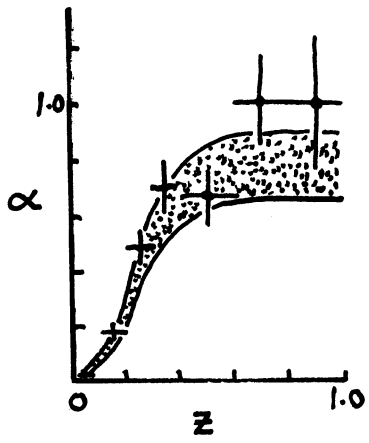

Fig. 32 Jet model and data at 7.4 GeV